Boundary Layer Dynamics and Cross-Equatorial Hadley Circulation

OLIVIER PAULUIS

Department of Earth, Atmospheric, and Planetary Sciences, Massachusetts Institute of Technology, Cambridge, Massachusetts

(Manuscript received 9 May 2003, in final form 12 November 2003)

ABSTRACT

The behavior of the Hadley circulation is analyzed in the context of an idealized axisymmetric atmosphere. It is argued that the cross-equatorial Hadley circulation exhibits two different regimes depending on the depth of the planetary boundary layer and the sea surface temperature gradient in the equatorial regions. The first regime corresponds to a classic direct circulation from the summer to winter hemisphere. The second regime differs in that the return flow rises above the boundary layer in the winter hemisphere and crosses the equator within the free troposphere. This equatorial jump is associated with a secondary maximum in precipitation on the winter side of the equator.

The transition between these two regimes can be understood through the dynamical constraints on the low-level flow. Strong virtual temperature gradients are necessary for the return flow to cross the equator within the planetary boundary layer. However, the mass transport driven by such a temperature gradient is highly sensitive to the thickness of the boundary layer. For a weak temperature gradient or a shallow boundary layer, the return flow is prevented from crossing the equator within the the boundary layer and, instead, must do so in the free troposphere. These dynamical constraints act equally in a dry and a moist atmosphere. However, a comparison between dry and moist simulations shows that the equatorial jump is much deeper in a moist atmosphere. This is interpreted as resulting from the feedbacks between the large-scale flow and moist convection, which results in establishing a very weak gross moist stability for the equatorial jump.

1. Introduction

The two Hadley cells are a dominant feature of the zonally averaged circulation. During fall and spring, air ascends in the equatorial regions, moves poleward in the upper troposphere, subsides in the subtropics, and flows back toward the equator in the lower troposphere. At the solstice, the ascent regions shift into the summer hemisphere, and the cross-equatorial branch of the circulation intensifies significantly. This overturning circulation carries heat, momentum, and water vapor, and, by doing so, changes the wind, temperature, and humidity distribution of the tropical atmosphere.

In the Tropics, the atmospheric circulation is closely tied to precipitation. When moist air ascends, its temperature drops, and water vapor condenses and precipitates. The ascending branch of the Hadley circulation thus corresponds to regions of intense, deep convection of the intertropical convergence zone (ITCZ). Understanding the distribution of precipitation remains an important question in climate science. General circulation models (GCMs) usually have difficulties reproducing the observed precipitation pattern as well as its variability. From a theoretical perspective, it is usually considered that precipitation is controlled mostly by the sea surface temperature (SST) distribution (Lindzen and Nigam 1987).

This paper argues that, in addition, the meridional overturning circulation also plays a significant role in determining the distribution of precipitation. An axisymmetric model is used to investigate dynamical constraints on low-level circulation and their impact on the precipitation. The planetary boundary layer (PBL), that is, the region of the lower atmosphere that is directly affected by surface friction and energy fluxes, is of particular interest when considering the relationship between circulation and precipitation. There are two reasons for this. First, evaporation at the earth's surface is the primary energy source for the atmosphere. However, the latent heat of vaporization is only released when water vapor condenses. Since the lower troposphere contains most of the atmospheric water vapor, the transport of water vapor, and thus of latent heat, is dominated by the low-level flow. Second, since the PBL feels the effect of surface friction, its dynamical behavior is different from the upper troposphere, which can be viewed as mostly inviscid. Hence, the dynamics of the PBL flow can affect water vapor transport and precipitation.

It is shown here that there are two distinct regimes for the cross-equatorial Hadley circulation. The first re-

Corresponding author address: O. Pauluis, NOAA/GFDL, Princeton Forrestal Campus, U.S. Rte. 1, P.O. Box 308, Princeton, NJ 08542-0308.
E-mail: pauluis@princeton.edu

gime is a classic direct circulation, with the ITCZ located over the warm SST and subsidence in the winter hemisphere. The second regime exhibits a horseshoe-like circulation where the return flow of the Hadley circulation rises above the PBL in the winter hemisphere, crosses the equator within the free troposphere, and subsides on the summer side before reaching the main ascending regions. This equatorial jump is associated with a second maximum in the winter hemisphere. The transition between these two regimes is primarily controlled by dynamical constraints on the PBL flow.

The Hadley circulation is discussed here in the context of an idealized axisymmetric model. Midlatitude eddies extend the mass, heat, momentum, and water transports from the subtropics into the midlatitudes and polar regions. Because of this, the Hadley circulation can only be fully understood in connection with midlatitude weather systems. Nevertheless, axisymmetric models of the atmosphere, which cannot account for the effects of the eddies, have proven to be quite successful at providing insights into the behavior of the Hadley circulation. Such axisymmetric models have been used by several authors to investigate the behavior of the Hadley cell. Schneider (1977) points out the importance of advection of angular momentum in determining the response of an axially symmetric atmosphere to heat sources in the Tropics. Held and Hou (1980) show that a nonlinear, angular-momentum conserving circulation is present in the limit of vanishing viscosity. This axisymmetric Hadley cell is confined to the subtropics while the rest of the atmosphere is in radiative–convective equilibrium. However, the mass transport obtained in Held and Hou (1980) is significantly weaker than that indicated by observations (see, e.g., Peixoto and Oort 1992). Lindzen and Hou (1988) show that a small displacement of the heat source away from the equator produces a much stronger cross-equatorial circulation. This leads to a description of the annual-mean Hadley circulation as resulting from the averaging of two strong cross-equatorial cells. Interestingly, the intensity of the circulation obtained in Lindzen and Hou (1988) is similar to that of the observed Hadley circulation. That an axisymmetric model produces realistic behavior might be explained in part by the fact that, around the solstice, easterly winds shield the equatorial regions from the influence of midlatitude disturbances. Hence, despite their inherent limitations, studies of idealized cross-equatorial axisymmetric Hadley cells provide a good basis for investigating the overturning large-scale circulation in the equatorial regions.

This paper focuses on the dynamical feedbacks between the large-scale overturning circulation and the meridional distribution of precipitation. Previous investigations with axisymmetric models have mostly relied on dry thermodynamics: latent heat release is accounted for only as part of the prescribed external forcing, but there is no dynamic treatment of water vapor. Such studies have shown that the behavior of the Hadley circulation is highly sensitive to the location of precipitation (Lindzen and Hou 1988), and to its meridional extent (Hou and Lindzen 1992). Some results for dry circulation have already been extended to a moist atmosphere, such as Numaguti (1993), Satoh (1994), and Emanuel et al. (1994), who derive the equivalent to the Held and Hou criterion for a moist atmosphere. It remains that to obtain a self-consistent theory of the Hadley circulation, one must address the issue of how the large-scale flow affects the latitudinal distribution of precipitation.

The potential temperature tendency can be written as

$$\frac{d\theta}{dt} = \dot{\theta}_{\text{cnv}} + f_{\text{rad}}. \tag{1}$$

Here, θ is the potential temperature, f_{rad} is the radiative forcing, and $\dot{\theta}_{\text{cnv}}$ is the convective heating rate. In Held and Hou (1980), these two terms are replaced by a relaxation toward a prescribed radiative–convective equilibrium temperature:

$$\frac{d\theta}{dt} = \alpha(\theta_E - \theta). \tag{2}$$

Here, θ_E is the potential temperature in radiative–convective equilibrium as a function of height and latitude and α^{-1} is the relaxation time scale. The Newtonian cooling $\alpha(\theta_E - \theta)$ can be viewed as an ad hoc parameterization for radiative cooling. It is more difficult to justify its use for latent heat release. It is still possible to choose the radiative-equilibrium temperature distribution in such a way as to reproduce some of the effects of latent heating, for example, by choosing θ_E to be close to a moist adiabat, and by reducing the relaxation time scale in regions of deep convection, such as in Fang and Tung (1996). In this case, one can view a ''dry experiment'' as analyzing the atmospheric response to a prescribed distribution of precipitation. The drawback of this approach lies in that the dominant balance in Eq. (2) is between the vertical advection of potential temperature and the diabatic heating:

$$w\partial_z\theta \approx \alpha(\theta_E - \theta). \tag{3}$$

Because variations of θ are usually smaller than the variation of θ_E, this dominant balance (3) implies a very close relationship between vertical velocity (w) and θ_E. The structure of the overturning circulation can be, in most cases, directly determined from the meridional distribution of radiative–convective equilibrium temperature alone. In a moist atmosphere however, the large-scale flow transports water vapor and modifies the distribution of precipitation. This in turn changes the latent heat release and the overturning circulation. Such dynamical feedbacks affect not only the latitudinal distribution of precipitation, but can also modify the vertical distribution of the latent heat release.

The importance of the boundary layer for the Hadley

circulation has already been emphasized by previous studies. In Held and Hou (1980), the flow is divided into an upper-tropospheric, an angular-momentum-conserving branch, and a return flow in the lower troposphere. This return flow is directly affected by surface friction. It is argued in section 2 that this description is too simplistic and overlooks the possibility for part of the return to occur above the boundary layer. A key constraint here is that there must be a meridional pressure gradient within the PBL in order to balance the surface friction. In the equatorial regions, such a pressure gradient is mostly the result of a density gradient within the PBL, as argued by Lindzen and Nigam (1987). The return flow of the Hadley circulation can cross the equator in the PBL only if there is a strong enough cross-equatorial temperature gradient. Otherwise, the equator can act as a barrier for the return flow, which must then cross the equator within the free troposphere.

Section 3 shows that these dynamical constraints on the PBL flow can affect the distribution of precipitation. By varying the thickness of the PBL in a simple model, one can obtain two distinct regimes for the cross-equatorial Hadley circulation. The first regime, occurring for a thick PBL, corresponds to the ''classic'' Hadley circulation with a single overturning cell. Air rises over regions of warm SST in the summer hemisphere, crosses the equator near the tropopause, subsides in the subtropics of the winter hemisphere, and returns within the PBL. The second regime differs in that the return flow rises above the PBL in the winter hemisphere, crosses the equator in the free troposphere, and subsides in the summer hemisphere, giving the overturning circulation a horseshoe shape. This equatorial jump is associated with a secondary maximum of precipitation on the winter side of the equator.

Section 4 analyzes the differences between dry and moist Hadley circulations. While the dynamical constraints on the flow in the PBL are the same in a dry and a moist atmosphere, the feedbacks between circulation and precipitation modify how the atmosphere responds to the presence of this equatorial barrier. Section 5 discusses the implications of this work for the current understanding of the cross-equatorial circulation.

2. Theory

a. Model equations

An idealized axisymmetric model is constructed here to investigate the role of the PBL in the Hadley circulation. The atmosphere is divided vertically into two parts: a free atmosphere above and a PBL near the surface. For simplicity, the PBL is represented here as a mixed layer (ML) of constant depth, within which turbulence instantly homogenizes the horizontal momentum through the ML. As such, this ML is at best an ad hoc representation of the PBL. Nevertheless, this is enough to produce complex interactions with the Hadley circulation, as is illustrated in section 3.

In the free atmosphere, the equations for the angular momentum budget, meridional momentum budget, hydrostatic balance, and continuity can be written as

$$\frac{\partial M}{\partial t} + \frac{v}{a}\frac{\partial M}{\partial \phi} + w^*\frac{\partial M}{\partial z^*} = p^{-1}\frac{\partial}{\partial z^*}\nu p\frac{\partial M}{\partial z^*}, \quad (4)$$

$$\frac{\partial v}{\partial t} + \frac{v}{a}\frac{\partial v}{\partial \phi} + w^*\frac{\partial v}{\partial z^*} + \frac{u^2}{a}\tan\phi = -fu - \frac{1}{a}\frac{\partial \Phi}{\partial \phi} + p^{-1}\frac{\partial}{\partial z^*}\nu\frac{\partial pv}{\partial z^*}, \quad (5)$$

$$\frac{\partial \Phi}{\partial z^*} = \frac{RT_v}{H_r}, \quad \text{and} \quad (6)$$

$$\frac{1}{a\cos\phi}\frac{\partial}{\partial \phi}(pv\cos\phi) + \frac{\partial pw^*}{\partial z^*} = 0. \quad (7)$$

The vertical coordinate used here is log pressure defined as $z^* = H_r \ln(pr/p)$, where H_r is an arbitrary reference height, usually taken to the reference-scale height RT/g and p_r is a reference pressure taken here to be the average surface pressure. The vertical velocity is $w^* = dz^*/dt = -H_r(\omega/p)$, with ω the rate of change of pressure, and u and v are the zonal and meridional wind. The pressure $p = p_r \exp(-z^*/H_r)$ acts as the density in log pressure coordinates. The angular momentum M is given by $M = \Omega a^2 \cos^2\phi + ua\cos\phi$, where Ω is the rotation rate of the earth, a is its radius, ϕ is the latitude, $f = 2\Omega\sin\phi$ is the local value Coriolis parameter, and ν is the viscosity. The geopotential height is Φ, and $T_v = T[1 + (R_v - R_d)/R_d]$ is the virtual temperature, with R_d and R_v the gas constants for dry air and water vapor, and r the mixing ratio of water vapor.

The ML layer is treated here as a single layer of constant thickness in which the zonal and meridional winds are constant. The index b refers to the value of a variable within the ML, while the index f refers to a variable in the free troposphere right above the ML. Hence, u_b, v_b, and M_b are, respectively, the zonal wind, meridional wind, and angular momentum in the ML, while u_f, v_f, and M_f are the values of the same variables measured right above the ML.

The angular momentum tendency can be obtained by integrating (4) between the surface and the top of the ML, and assuming that the viscous flux vanishes at the top of the ML. This yields

$$\frac{\partial M_b}{\partial t} + \frac{v_b}{a}\frac{\partial M_b}{\partial \phi} + \frac{p_b w_b^*}{H_r \Delta P}(M_f - M_b) = \frac{\mathcal{F}_{M,0}}{H_r \Delta P}. \quad (8)$$

Here, w_b^* is the vertical velocity at the top of the ML. (Note that w is still a function of height within the ML.) The pressure thickness of the ML is $\Delta P = p_0 - p_b$ and is assumed to be constant, with p_b the pressure at the top of the ML. The surface flux of the angular momentum is $\mathcal{F}_{M,0}$, and it is assumed that the momentum flux vanishes at the top of the ML.

The ML momentum budget in the meridional direction is derived by integrating (5):

$$\frac{\partial v_b}{\partial t} + \frac{v_b}{a}\frac{\partial v_b}{\partial \phi} + \frac{u_b^2}{a}\tan\phi + \frac{p_b w_b^*}{H_r \Delta P}(v_f - v_b) = -fu_b - \frac{1}{a}\frac{\partial \Phi}{\partial \phi}\bigg|_b + \frac{\mathcal{F}_{v,0}}{H_r \Delta P}. \quad (9)$$

The terms on the left-hand side are, respectively, the time tendency, meridional advection, spherical geometry term, and vertical advection of meridional momentum. The first term on the right-hand side accounts for the Coriolis acceleration through the ML, the second term, $\partial\Phi/\partial\phi|b$, is the geopotential gradient averaged over the ML, and the third term is the surface friction.

The geopotential gradient at any level z^* in the ML can be obtained by integrating the hydrostatic relationship (6) from the top of the ML to the level p:

$$\frac{\partial \Phi}{\partial \phi}(z^*) = \frac{\partial \Phi}{\partial \phi}(\Delta H) - \int_{z^*}^{\Delta H} \frac{R}{H_r}\frac{\partial T_v}{\partial \phi}\, dz^*. \quad (10)$$

In the free troposphere, right above the ML, the flow can be assumed to be in geostrophic balance. This yields

$$\frac{1}{a}\frac{\partial \Phi}{\partial \phi}(\Delta H) = -fu_f, \quad (11)$$

with u_f the zonal velocity right above the ML. Hence, the averaged geopotential gradient within the ML can be approximated by

$$\frac{1}{a}\frac{\partial \Phi}{\partial \phi}\bigg|_b = -fu_f - \frac{\Delta H}{2H_r}\frac{R}{a}\frac{\partial T_v}{\partial \phi}, \quad (12)$$

where it has been assumed that the virtual temperature gradient is constant through the mixed layer. The geopotential gradient can thus be decomposed as the sum of the gradient at the top of the ML and a contribution of the virtual temperature gradient.

These dynamical equations are completed by equations for potential temperature and water vapor. The tendency for the potential temperature θ is given by

$$\frac{\partial \theta}{\partial t} + \frac{v}{a}\frac{\partial \theta}{\partial \phi} + w^*\frac{\partial \theta}{\partial z^*} = \dot{\theta}_{\text{cnv}} + f_{\text{rad}}, \quad (13)$$

where f_{rad} represents the change in potential temperature due to radiative cooling. For simplicity, the potential temperature tendencies due to deep and shallow convection are gathered into a single term $\dot{\theta}_{\text{cnv}}$. The water vapor budget is written as

$$\frac{\partial r}{\partial t} + \frac{v}{a}\frac{\partial r}{\partial \phi} + w^*\frac{\partial r}{\partial z^*} = \dot{r}_{\text{cnv}}, \quad (14)$$

with $\dot{r}_{\text{cnv}}$ the change due to convection.

To solve the set of equations (4)–(14), it is necessary to specify the surface fluxes, the radiative cooling rate f_{rad}, and the convective tendencies $\dot{r}_{\text{cnv}}$ and $\dot{\theta}_{\text{cnv}}$. The surface fluxes are obtained from a bulk formulation:

$$\mathcal{F}_{M,s} = C_D p_0 |\mathbf{V}_0|(M_s - M_b), \quad (15)$$

$$\mathcal{F}_{v,s} = C_D p_0 |\mathbf{V}_0|(v_s - v_b), \quad (16)$$

$$\mathcal{F}_{r,s} = C_k p_0 |\mathbf{V}_0|(r_s^* - r_0), \quad \text{and} \quad (17)$$

$$\mathcal{F}_{\theta,s} = C_k p_0 |\mathbf{V}_0|(\theta_s - \theta_0). \quad (18)$$

Here, $\mathcal{F}_{M,s}$, $\mathcal{F}_{v,s}$, $\mathcal{F}_{r,s}$, and $\mathcal{F}_{\theta,s}$ are the fluxes of angular momentum, meridional momentum, water vapor, and sensible heat at the lower boundary, and C_D and C_k are the bulk dynamic and thermodynamic coefficients. Variables with an index s correspond to quantities measured at the earth's surface, with r_s^* being the saturation water vapor mixing ratio at the surface temperature and pressure. The index 0 refers to quantities measured close to the surface, usually at a reference height of 10 m. The surface velocity $|\mathbf{V}_0|$ is given by $|\mathbf{V}_0| = (u_b^2 + v_b^2 + w_c^2)^{1/2}$, where w_c is the gustiness associated with low-level turbulence.

b. The inviscid limit

Because the molecular viscosity of air is very small, one can first consider the case $\nu = 0$ and $\Delta H = 0$. Held and Hou (1980) consider a first solution to (4)–(14) in which the atmosphere is in local radiative–convective equilibrium (RCE). This solution is characterized by (a) a balance between radiative cooling and convective heating $f_{\text{rad}} + \dot{\theta}_{\text{cnv}} = 0$, (b) the absence of any circulation $v = \omega = 0$, and (c) the zonal wind in gradient wind balance.

However, the viscosity of the air, while small, is not zero. Instead of the case $\nu = 0$, one should study the inviscid limit, that is, the lim $\nu \to 0^+$ of an infinitesimally small viscosity. Held and Hou (1980) argue that the RCE solution can be singular; that is, the viscous solution does not converge toward the RCE solution for $\nu \to 0^+$. In a steady flow in a viscous, axisymmetric atmosphere, any local extrema of angular momentum must be located at the lower boundary of the domain. The RCE solution is singular when the RCE temperature distribution presents a horizontal gradient larger than a certain threshold. In this case, the inviscid limit differs from the the RCE solution by the presence of an overturning circulation. This circulation is limited to a specific portion of the atmosphere, outside which the RCE solution still applies. In the simplest cases, the circulation consists of two Hadley-like overturning cells in the Tropics. It redistributes angular momentum and energy and, by doing so, maintains the temperature and humidity distributions in these regions away from the local radiative–convective equilibrium. As long as the meridional velocity remains small, the meridional momentum budget (5) can be approximated by the gradient wind balance, and the temperature distribution can be derived from the zonal wind profile through the thermal wind relationship.

In the inviscid limit, angular momentum is conserved

away from a thin surface layer at the lower boundary. The tropopause is determined by the trajectory of the highest reaching parcel, and corresponds to a surface of constant angular momentum. More generally, all streamlines of the circulation in the free troposphere are also surfaces of constant angular momentum.

At the lower boundary, the angular momentum is modified by surface friction. However, in the absence of a mixed layer, the friction is only felt through a thin surface layer of thickness proportional to $\nu^{1/2}$. In the inviscid limit, the surface layer thickness is only an infinitesimal portion of the atmosphere, and surface friction can only affect a very small fraction of the flow. Hence, angular momentum is almost conserved in the return flow. For a steady circulation, Fang and Tung (1996) show that the angular momentum would be homogenized within any regions with an overturning circulation, and the thermal wind relationship implies that there is no horizontal temperature gradient within these regions. As the boundary between the overturning cell and the rest of the atmosphere also corresponds to a parcel trajectory, it is also characterized by a discontinuity in angular momentum. This also implies a discontinuity in temperature because of the hydrostatic and gradient wind balance: the edge of the Hadley cell behaves as a sloping front.

The ''purely'' inviscid limit in which the viscosity goes uniformly to 0 through the whole atmosphere is not the most relevant for the earth's atmosphere. Indeed, turbulence and shallow convection continuously mix angular momentum through the planetary boundary layer. Held and Hou (1980) actually consider this alternative limit and not the purely inviscid limit in their discussion of the return flow. The inviscid limit corresponds to the case of taking simultaneously the limit of $\nu \to 0+$ and $\Delta H \to 0$.

c. Dynamical constraints on the flow in the mixed layer

For a weak overturning circulation, the equations can be linearized for a reference state at rest. For a steady flow, the linearized angular- and meridional-momentum equations (8) and (9) become

$$f v_b - \tau^{-1} u_b = 0 \quad \text{and} \tag{19}$$

$$f u_b + \frac{1}{a}\frac{\partial \Phi}{\partial \phi}\bigg|_b + \tau^{-1} v_b = 0, \tag{20}$$

where τ is a frictional dissipation time scale given by

$$\tau = \frac{H_r \Delta p}{p_0 C_d |w_c|}. \tag{21}$$

The zonal and meridional wind distribution can be obtained from (19), (20) for a given meridional geopotential gradient:

$$u_b = \frac{\tau^2}{f}(1 + f^2\tau^2)\frac{\partial \Phi}{\partial \phi}\bigg|_b \quad \text{and} \tag{22}$$

$$v_b = \tau(1 + f^2\tau^2)\frac{\partial \Phi}{\partial \phi}\bigg|_b. \tag{23}$$

The decomposition of the geopotential gradient between a free-tropospheric contribution and a temperature contribution (12) yields a similar decomposition for the meridional velocity:

$$v_b = v_w + v_T. \tag{24}$$

Here, v_T is the meridional flow induced by a temperature gradient within the ML:

$$v_T = \tau(1 + f^2\tau^2)^{-1}\frac{\Delta H}{2H_r}\frac{R}{a}\frac{\partial T_v}{\partial \phi}. \tag{25}$$

Similarly, v_w is the boundary layer flow driven by the geopotential gradient in the free troposphere and is directly related to the zonal wind u_f right above the ML, with

$$v_w = f\tau(1 + f^2\tau^2)^{-1} u_f. \tag{26}$$

The zonal wind in the free troposphere is constrained by angular momentum conservation. The angular momentum of an air parcel in the free troposphere must be between the angular momentum of the solid-body rotation in the ascent region and the corresponding value at the equator. If the large-scale ascent is localized at latitude ϕ_0, the zonal wind is bound by

$$\frac{a\Omega(\cos^2\phi_0 - \cos^2\phi)}{\cos\phi} < u_f(\phi) < \frac{a\Omega \sin^2\phi}{\cos\phi}, \tag{27}$$

for $|\phi| \le |\phi_0|$. This constraint on the zonal wind also implies upper and lower bounds on pressure gradients in the free troposphere and, through Eq. (26), on the magnitude of the meridional circulation that the free-tropospheric pressure gradient can generate in the ML.

In the absence of a temperature gradient, the ML flow is driven solely by the free-tropospheric pressure gradient. In this case, an equatorward wind in the ML requires an equator-to-pole pressure gradient, and is associated with easterly wind in the free troposphere, as indicated by (26). A bound on equatorward velocity is obtained by taking the lower bound for u_f in (27), that is, by assuming that the wind in the free troposphere has the angular momentum of the solid-body rotation in the ascending regions. This yields

$$|v_w| \le 2a\Omega^2\tau(\cos^2\phi_0 - \cos^2\phi)\tan\phi. \tag{28}$$

This upper bound is proportional to the local value of the Coriolis parameter and decreases linearly to 0 at the equator. Similarly, a poleward flow requires a westerly wind in the free troposphere. An upper bound on the poleward velocity in the ML is obtained by taking the upper bound for u_f in (27), that is by assuming that the

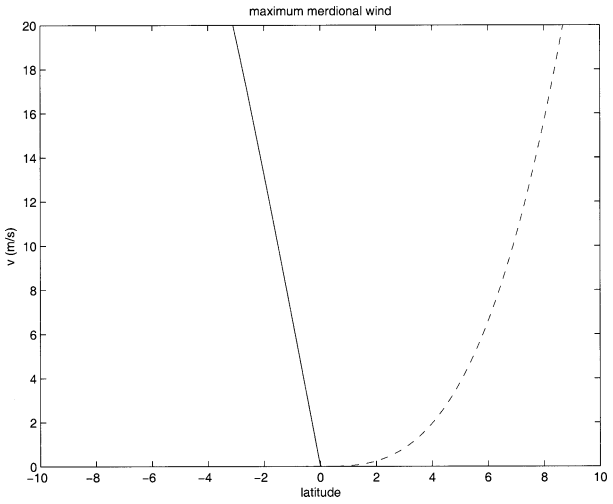

FIG. 1. Maximum meridional velocity driven by a free pressure tropospheric gradient for an ML thickness of a damping time scale of $\tau = 1$ day and the ascent regions located at 15°N. The upper bound on the meridional wind is given by (28) for the equatorward flow (solid line, south of the equator) and by (29) for the poleward flow (dashed line, north of the equator).

wind in the free troposphere has the angular momentum of the solid-body rotation at the equator:

$$|v_w| \leq 2a\Omega^2\tau \frac{\sin^3\phi}{\cos\phi}. \tag{29}$$

The upper bound on the poleward flow is proportional to the third power of the distance from the equator. The asymmetry between equatorward and poleward flow is a direct consequence of angular momentum conservation imposing different constraints on easterly and westerly winds.

In the absence of temperature gradients, the magnitude of the meridional wind is bounded by (28) and (29). These constraints are illustrated in Fig. 1 for a hypothetical flow with the ascent regions located at $\phi_0 = 15°$N and a frictional dissipation time of $\tau = 1$ day. These bounds are due to the fact that geopotential gradients in the free troposphere are particularly weak in the equatorial regions and are, therefore, inefficient at driving a cross-equatorial flow in the ML. The flow illustrated in Fig. 1 is associated with ascending motion on the winter side of the equator and weak subsidence on the summer side. Notice that such a flow also requires the wind in the free troposphere to be easterly on the winter side of the equator and westerly on the summer side. Such a change in the wind pattern can only occur if there is some ascent in the equatorial regions.

Temperature gradients in the ML generate a flow from the colder regions to the warmer regions, as indicated by (25), and can drive a cross-equatorial flow within the ML. There are thus two possible situations. On the one hand, a strong enough temperature gradient or thick enough ML can generate sufficient cross-equatorial geopotential gradient for the return flow to occur within the ML. On the other hand, for a weak temperature gradient or a thin ML, the temperature driven cross-equatorial flow is smaller than the ML flow in the subtropics, and a large fraction of the return flow must rise above the ML in the winter hemisphere and cross the equator in the free troposphere.

A uniform temperature gradient within the ML results in a geopotential gradient proportional to the ML thickness. Equations (25) and (21) indicate that the corresponding meridional wind would be proportional to the square of the ML thickness and, therefore, that the ML mass transport is proportional to the third power of the mixed layer depth. As the cross-equatorial mass transport is primarily due to the temperature gradient, one expects thus that a portion of the return flow that crosses the equator within the ML will be highly sensitive to the PBL depth in the equatorial regions.

The constraints on the return flow have been derived from the linearized momentum budgets (19)–(20) in which the dominant balance is between the meridional pressure gradient and surface friction. For a strong enough circulation, advection might change the behavior of the flow. Horizontal advection of meridional momentum has a limited impact as long as the ML wind remains small (of the order of a few meters per second). For earthlike conditions, it is insufficient to drive a significant cross-equatorial flow. Advection of angular momentum only affects the angular momentum budget and cannot by itself generate a meridional acceleration of the flow. Entrainment may potentially drive a circulation in the ML. It is, however, limited to regions with large-scale subsidence and drives an ML flow in the same direction as the flow in the free troposphere. The corresponding meridional velocity is proportional to

$$v_{b,e} \approx \frac{\tau}{\tau_e + \tau} v_f, \tag{30}$$

with $\tau_e = H_r\Delta P/(p_b w_b)$ a subsidence time scale and v_f the meridional wind in the free troposphere. As the subsidence time scale is much smaller than the frictional time scale, $\tau_e \ll \tau$, entrainment can only drive an ML circulation that is much weaker than the corresponding circulation in the free troposphere. Hence, although entrainment may have a significant impact on the ML flow, the flow that is generated this way will always be small in comparison to the circulation in the free troposphere.

Although this discussion has been primarily concerned with the cross-equatorial flows, the constraints on the mixed layer flow also have implications for a Hadley circulation centered at the equator. For air rising at the equator, conservation of angular momentum indicates that westerlies will be present in the free troposphere. Hence, the equator corresponds to an area of high geopotential, preventing an equatorward circulation in the ML. Most of the axisymmetric Hadley circulation, including the return flow, will occur in the free troposphere. A circulation can exist within the ML if

either strong temperature gradients are present in the ML, or if there is strong enough easterly wind in the free troposphere. This, however, requires a significant exchange of momentum between the Tropics and extratropics (e.g., due to the action of baroclinic eddies). In the context of an axisymmetric model, this suggests that the equatorially centered Hadley cell is much wider in the upper troposphere than near the surface, as is apparent in the simulations of Held and Hou (1980), and that the low-level flow is highly sensitive to the angular momentum exchange at the edge of the Hadley cell.

3. Numerical model

The sensitivity of the cross-equatorial Hadley circulation to the mixed layer depth is investigated in a set of numerical experiments. The model used here has been developed in collaboration with S. Bony at the Massachusetts Institute of Technology (MIT) and is similar to that used in Pauluis and Emanuel (2004). The dynamical core is based on the MITGCM (Hill and Marshall 1995; Marshall et al. 1997; Adcroft et al. 1999). Convective energy and water vapor transports are obtained by using the convective parameterization of Emanuel and Zivkovic-Rothman (1999). To remain as close as possible to the inviscid limit, the viscosity and diffusivity are kept as small as possible (100 $Pa^2\ s^{-1}$), and the convective transport of momentum has been removed from the convective parameterization, in order to remain as close as possible to the theoretical inviscid limit. Tests with the convective transport of momentum did not differ significantly from the results presented here. A numerical fourth-order Shapiro filter is used in the horizontal directions in order to remove numerical noise at small scales. Surface fluxes are given by the bulk formulas (15)–(18), using $C_D = C_k = 1.210^{-3}$ m s^{-1}, and the gustiness is $w_c = 4$ m s^{-1}, while the SST is prescribed as a function of the latitude: $T_S = T_0 + \Delta T \cos^2[0.5\pi(\phi - \phi_0)/\Delta\phi]$ for $\phi_0 - \Delta\phi < \phi < \phi_0 + \Delta\phi$, and $T_s = T_0$ elsewhere. The values used in the experiments discussed below are $T_0 = 298.15$ K, $\Delta T = 4$ K, and $\Delta\phi = 15°$. The SST maximum is localized at $\phi_0 = 15°$N (for the experiments shown in Figs. 3–5), at $\phi_0 = 10°$N (for the experiment in Fig. 7, and $\phi_0 = 20°$ for the experiment in Fig. 8). These SST distributions are illustrated in Fig. 2. This SST distribution has a maximum in the tropical regions, while being constant in the extratropics. This distribution violates the Held and Hou criterion generalized for a moist atmosphere (see Emanuel et al. 1994), so as to produce an axisymmetric overturning circulation. The troposphere is cooled by using a Newtonian relaxation: temperature is relaxed toward an ''equilibrium'' value given by $T_e = \min(240 - p/100, 200)$ K, with p expressed in hectopascals. The relaxation time scale is 40 days. This Newtonian cooling produces a fairly homogeneous radiative cooling of approximately 1 K day^{-1} throughout the troposphere and maintains the stratosphere at a constant temperature of 200 K. Notice that the Newtonian cooling is independent of the latitude, so that the presence of a circulation results only from the variations of SST. In the mixed layer, the horizontal velocities are homogenized over a time scale of 20 min. The vertical mixing does not affect the thermodynamical variables (potential temperature and water vapor). This has already been done within the convective parameterization. The mixed layer thickness ΔP is constant over the whole domain. The axisymmetric grid resolution is 25 hPa in the vertical direction and 1.5° in the latitudinal direction. The experiments are run for a period of 200 days, with only the last 100 days used for the diagnostics.

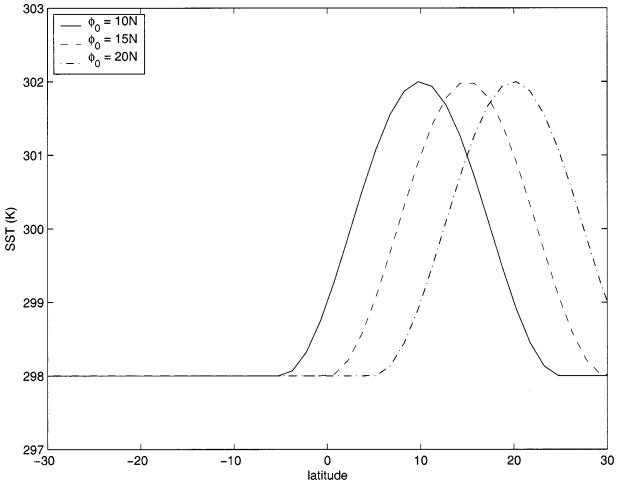

FIG. 2. SST distribution used in the numerical experiments. The experiments in Figs. 3–5 correspond to a maximum SST located at 15°N (dashed line), Fig. 7 to a maximum SST at 10°N (solid line), and Fig. 8 to a maximum SST at 20°N (dashed–dotted line).

To illustrate the transition between a thin and a thick layer, three cases are discussed here, for different mixed layer thicknesses of $\Delta P = 50$, 100, and 200 hPa respectively. The resulting circulations are shown in Figs. 3–5. The SST maximum off the equator is associated with very strong ascent and precipitation, corresponding to the ascending branch of a strong cross-equatorial Hadley circulation. The flow crosses the equator in the upper troposphere and subsides in the subtropics of the Southern Hemisphere, where the convective activity is suppressed. The intensity of the Hadley circulation, measured as the maximum streamfunction, appears not to be affected by the change in the ML depth.

The main difference occurs in the equatorial regions. The 200-hPa case corresponds to the classic view on the Hadley circulation, with the return flow taking place mostly within the ML. There is also a significant amount of precipitation between the equator and the SST maximum. In contrast, in both the 50- and the 100-hPa cases, the cross-equatorial Hadley circulation results in a strong return flow in the ML in the winter hemisphere. This return flow rises in the winter hemisphere, crosses

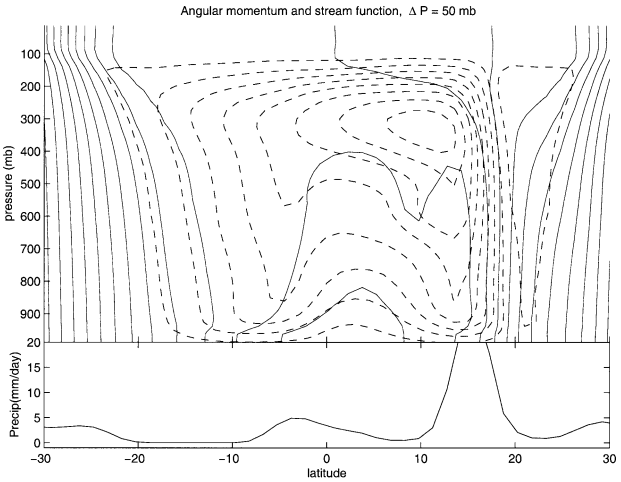

FIG. 3. (top) Angular momentum (solid line) and streamfunction (dashed line) for an ML depth of 50 hPa. Contour interval is 2% of the angular momentum of the solid-body rotation at the equator and 4×10^{11} kg s^{-1} for the streamfunction. (bottom) Precipitation (mm day^{-1}). Only the regions between 30°S and 30°N are shown.

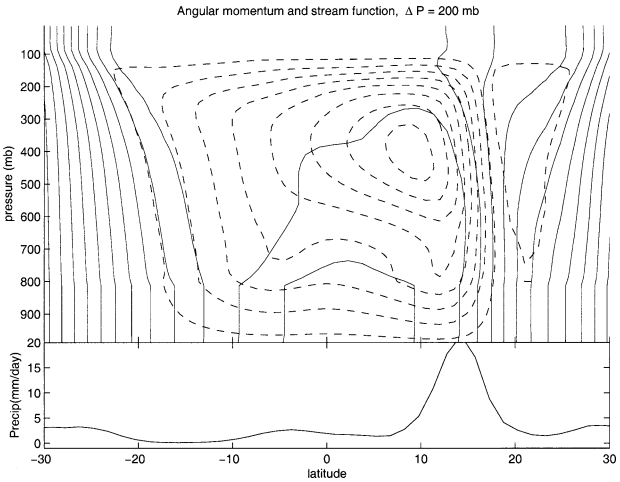

FIG. 5. Same as in Fig. 3 but for an ML depth of 200 hPa.

the equator within the free troposphere, and subsides in the summer hemisphere between the equator and the SST maximum. This equatorial jump is associated with a secondary maximum of precipitation. The presence of the secondary maximum of precipitation does not affect the main maximum over the warm SST.

Figure 6 shows the meridional velocity at the lowest level of the model (987.5 hPa). In the 50- and 100-hPa cases, there is a sharp drop of the meridional velocity in the equatorial regions. This drop of velocity is associated with the ascent regions on the winter side of the equator. Comparing Figs. 1 and 6 indicates that regions of weak meridional velocity correspond to the regions where the pressure gradient in the free troposphere is too weak to drive a strong flow in the ML. The regions of weak meridional wind are displaced slightly into the summer hemisphere, which is probably a result of the horizontal advection of the meridional momentum.

Two more experiments are presented in Figs. 7 and 8. In these experiments, the maximum SST is displaced to $\phi_0 = 10°$N (Fig. 7) and $\phi_0 = 20°$N (Fig. 8). In both cases, the mixed layer depth ΔP is 100 hPa, so that these experiments can be directly compared to that in Fig. 4. When the SST maximum is close to the equator so that there is a large SST gradient in the equatorial regions, a strong flow can cross the equator within the ML. Conversely, when the SST maximum is far away from the equator, and there is little SST gradient, the secondary maximum of precipitation is located farther away from the equator in the winter hemisphere, and the horseshoe-shaped character of the circulation is even more pronounced. The precipitation pattern in Fig. 8 is reminiscent of the precipitation pattern over the Indian Ocean during the northern summer, when a maximum

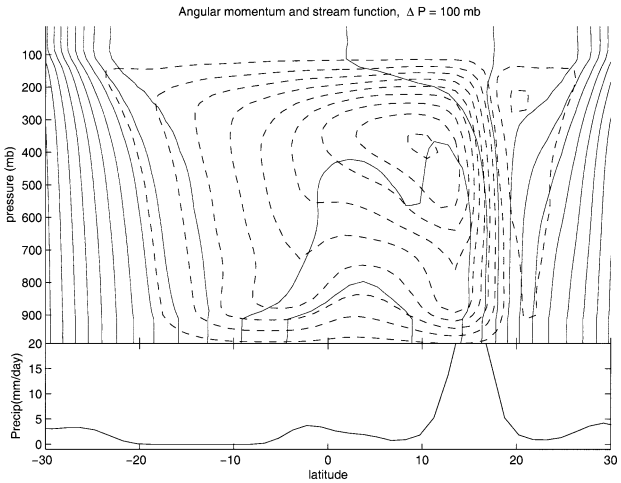

FIG. 4. Same as in Fig. 3 but for an ML depth of 100 hPa.

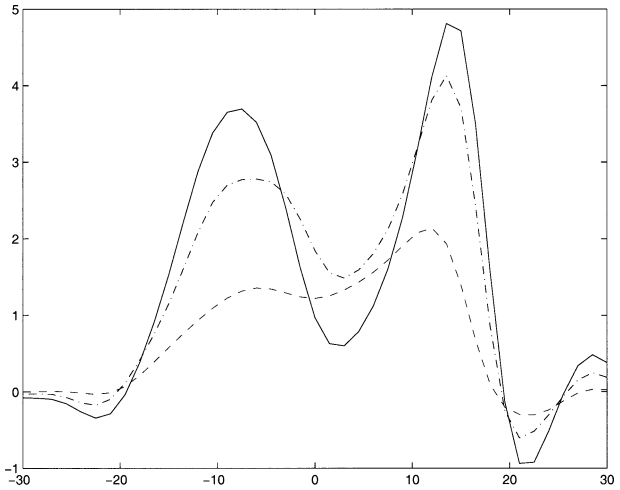

FIG. 6. Meridional wind velocity at 987.5 hPa for an ML depth of 50 (solid line), 100 (dashed–dotted line), and 200 hPa (dashed line).

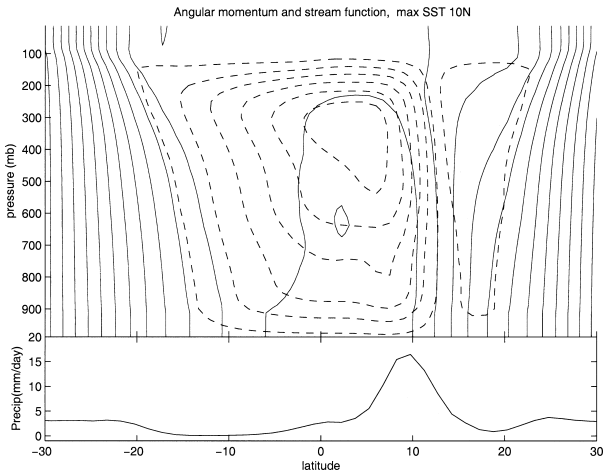

FIG. 7. Same as in Fig. 3 but for an ML depth of 100 hPa, and a maximum SST at 10°N.

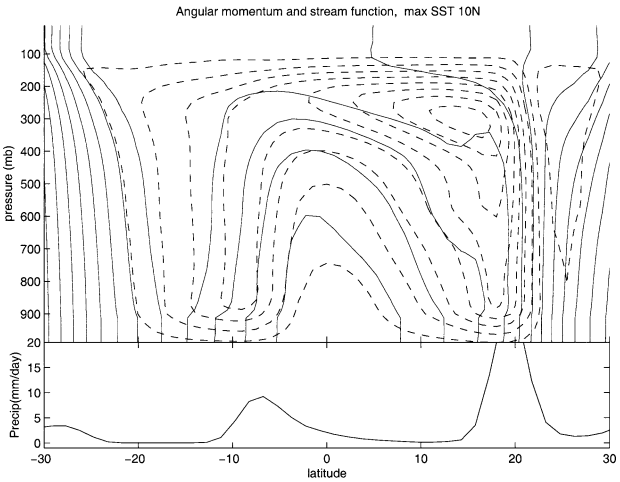

FIG. 8. Same as in Fig. 3 but for an ML depth of 100 hPa, and a maximum SST at 20°N.

of precipitation is present on the southern (winter) side of the equator.

Finally, to underline the differences between the dry and moist dynamics, an additional run is performed in which the moist dynamics are replaced by a simple relaxation toward the radiative–convective equilibrium profile. The radiative–convective equilibrium used here corresponds to the same SST distribution and the same Newtonian cooling as the moist simulations. The overturning for a ML depth of 50 hPa is shown in Fig. 9. An equatorial jump is also present in the dry simulation. However, while the jump in the moist case easily reaches the middle troposphere, the ascent is limited in the dry case, with air barely rising above the ML. A similar feature can be observed in the simulations presented by Plumb and Hou (1992).

4. Moist convection and equatorial ascent

The dynamical constraints on the PBL flow apply equally to dry and moist atmospheres. Indeed, both dry and moist simulations exhibit an equatorial jump. However, the ascent is much shallower in the dry circulation, barely rising above the PBL. The role of moist convection in strengthening and deepening the equatorial ascent is now discussed.

Consider first the dry case. The equatorial jump can be viewed as a small perturbation on a direct overturning cell for which all the return flow takes place in the ML. The discussion in section 2 indicates that the meridional pressure gradient can be insufficient to drive the cross-equatorial flow. Let us define F as the net, unbalanced, acceleration toward the winter hemisphere in the ML:

$$F = -f\overline{u}_b - \frac{1}{a}\frac{\partial\overline{\Phi}}{\partial\phi}\bigg|_b - \tau^{-1}\overline{v}_b. \tag{31}$$

One can compute the atmospheric response to a forcing F in the boundary layer. Assuming that the flow behaves linearly in the equatorial region, one can then view the atmospheric circulation as the superposition of a Hadley cell and an equatorial jump resulting from the excess surface friction at the lower boundary. For simplicity, the equations of motion [(4)–(7)] and the potential temperature equation (13) are linearized for a reference atmosphere at rest, and the spherical geometry is replaced by a beta-plane approximation. This yields

$$fv - \gamma u = 0, \tag{32}$$

$$-\partial_y\Phi' - fu = 0, \tag{33}$$

$$\partial_{z^*}\overline{\theta}w = -\alpha\theta', \tag{34}$$

$$\partial_{z^*}pw + \partial_y pv = 0, \quad \text{and} \tag{35}$$

$$\partial_{z^*}\Phi' = g^*\frac{\theta'}{\overline{\theta}}. \tag{36}$$

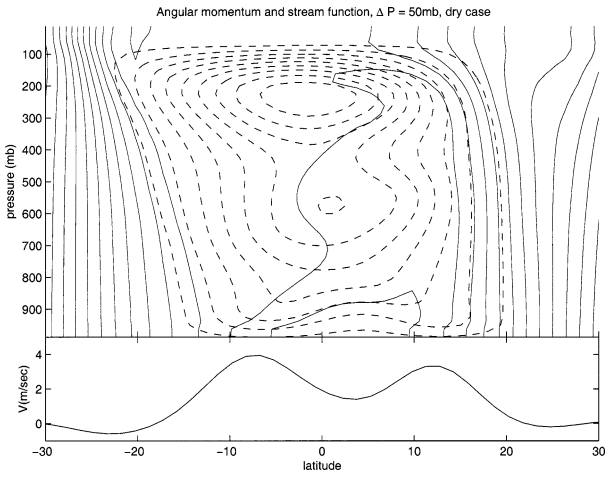

FIG. 9. (top) Angular momentum (solid line) and streamfunction (dashed line) for the dry experiment with an ML depth of 50 hPa. Contour interval is 2% of the angular momentum of the solid earth at the equator and 4×10^{11} kg s^{-1} for the streamfunction. (bottom) Meridional wind velocity at 987.5 hPa for an ML depth of 50 hPa.

The horizontal coordinate is the distance away from the equator $y = a \sin\phi$, so that the Coriolis parameter is $f = \beta y$. The perturbation geopotential is ϕ', while $\overline{\theta}$ is the potential temperature of the reference state. The quantity $g^* = \partial_{z^*}\overline{\Phi}$ is the vertical gradient of geopotential in the reference state. (In log pressure coordinates, it is not necessarily constant, but a proper choice of the reference height H_r can make it close to the gravitational acceleration.) A small damping term $-\gamma u'$ is included in the zonal momentum equation. This problem bears some similarities to the downward control of stratospheric circulation forced by a Rossby wave drag, as discussed, for example, by Plumb and Eluszkiewicz (1999). The main difference lies in the fact that the flow is forced by a meridional momentum forcing at the lower boundary instead of a zonal acceleration in the interior. As for the stratospheric flow, the drag on the zonal momentum is required to obtain a linear solution.

Equations (32)–(36) yield the PDE for Φ':

$$\frac{1}{p}\partial_{z^*} p \partial_{z^*}\Phi' + \frac{N^2\gamma}{\beta^2\alpha}\partial_y\left(\frac{1}{y^2}\partial_y p'\right) = 0, \qquad (37)$$

with $N^2 = g\partial_{z^*}\overline{\theta}/\overline{\theta}$ the Brunt–Väisälä frequency. The solution takes the form

$$p'(y, z) = \sum_n \exp\left(\frac{-z}{H_n}\right)\left[A_n y^{3/2} J_{3/4}\left(\frac{y^2}{2Y_n^2}\right) + B_n y^{3/2} J_{-3/4}\left(\frac{y^2}{2Y_n^2}\right)\right], \qquad (38)$$

with $J_{-3/4}$ and $J_{3/4}$ the Bessel function of order $-3/4$ and $3/4$. The partial differential equation (37) implies the relationship between the horizontal and vertical scales:

$$H_n = \left(\frac{H_r + H_n}{H_r}\right)^{1/2}\frac{\beta}{N}\left(\frac{\alpha}{\gamma}\right)^{1/2} Y_n^2. \qquad (39)$$

The lower-boundary condition is obtained by requiring that the net acceleration in the boundary layer is balancing the excess friction (31). This yields

$$-F = \frac{\partial p'(\Delta H)}{\partial y} + \tau^{-1}(1 + f^2\tau^2)\frac{\Psi(\Delta H)}{\Delta H}, \qquad (40)$$

where $\Psi(z) = \int_z^\infty v'\, dz$ is the streamfunction. The solution can be computed analytically as an expansion in the horizontal modes. Assuming that the meridional boundaries are far enough from the regions of the forcing, the atmospheric response is dominated by eigenmodes with a meridional extent similar to that of the forcing. For the equatorial jump, taking $Y_n \approx 500$ km, $N \approx 10^{-2}\ s^{-1}$, $H_r \approx 8$ km, and $\alpha/\gamma \approx 1$ yields a vertical scale height of approximately 250 m. The equatorial jump is shallow in the case of a strongly stratified dry atmosphere.

In a moist atmosphere, the adiabatic cooling in the ascent regions is partially compensated for by latent heat release. This can be viewed as a reduction of the gross moist stability of the atmosphere. Replacing the dry static stability by a weaker gross moist stability $N_{\text{eff}}^2 < N^2$ in (34) indicates the equatorial jump in a moist atmosphere would be deeper by a factor of N/N_{eff}.

What is the gross moist stability for the equatorial jump? The exact answer depends on the assumptions made about the behavior of convection. Different lines of arguments (Neelind and Held 1987; Emanuel et al. 1994; Yu et al. 1998) as well as observations (Wheeler and Kiladis 1999) indicate that the gross moist stability for a moist convective–gravity wave should be approximately one-tenth of the dry static stability: $N_{\text{eff}}^2 \approx 0.1N^2$. This corresponds to an equatorial jump about three times deeper in a moist atmosphere than in a dry atmosphere, all else being equal, and one would expect the flow to rise about 1 km or so above the ML. One might, however, question whether the gross moist stability of the equatorial jump should be similar to that observed in convective gravity waves, as the large-scale forcing producing the equatorial jump differs from the forcing on convective gravity waves both in terms of its frequency and its vertical structure. Comparing the dry and moist simulations indicates indeed that the moist equatorial jump is consistent with a gross moist stability much lower than that of convective–gravity waves.

One approach to determining the effective stratification is to analyze the energy budget of the convective regions. The meridional energy transport by an atmospheric flow is given by

$$E = \int_0^{p_{\text{surf}}} v(C_p T + L_v q + gz + \text{ke})\frac{dp}{g}, \approx \int_0^{p_{\text{surf}}} vh\frac{dp}{g}, \qquad (41)$$

where $C_p T + L_v q$ is the enthalpy of moist air, including the latent heat of vaporization, and $\text{ke} = 1/2(u^2 + v^2 + w^2)$ is the kinetic energy. In the equatorial regions, the transport of kinetic energy can generally be neglected and the energy transport is, to a very good approximation, equal to the transport of moist static energy $h = C_p T + L_v q + gz$.

A key feature of the tropical atmosphere is the presence of a minimum of moist static energy around 500–600 hPa. The existence of this minimum can be understood from the fact that, although the temperature of the tropical atmosphere is very close to that of a moist adiabat, the middle troposphere is far from saturation, and its moist static energy is thus lower than that of either the boundary layer or that of the upper troposphere. Consider a steady flow ascending from the PBL to some level in the lower troposphere, below the minimum of moist static energy. Such flow would result in a net convergence of moist static energy into the column. If this flow is perturbed so that the ascent is reinforced, this would reinforce the energy transport into

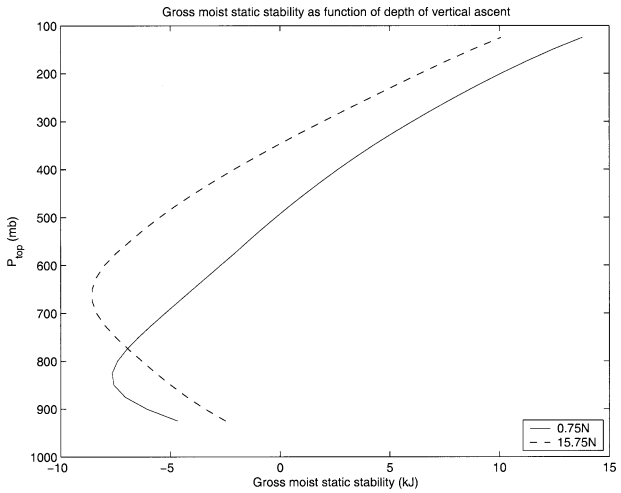

FIG. 10. Estimate of the gross moist static stability as a function of the depth of the ascent at 0.75° (solid line) and 15.75°N (dashed line). The gross moist static stability is obtained by using the moist static energy profile from the moist experiment with an ML thickness of 100 hPa.

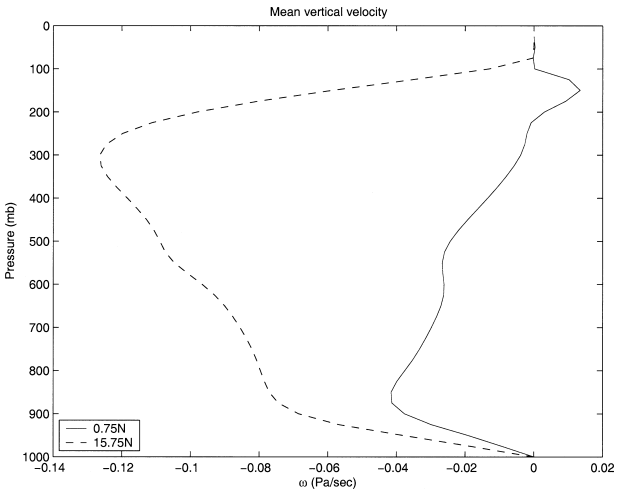

FIG. 11. Vertical velocity at 0.75° (solid line) and 15.75°N (dashed line) for an ML thickness of 100 hPa.

the ascent region. *If this inflow of energy results in an actual increase in temperature*,[1] then this temperature change produces a pressure gradient that reinforces the initial perturbation. A flow that results in an energy convergence into the ascending regions would be unstable to small perturbations. A stable flow requires the air to rise above the minimum of the moist static energy, so that the circulation exports heat from the ascending regions.

The energy export by the circulation in an atmospheric column can be approximated by

$$\frac{\partial E}{\partial y} \approx S = \int_{p_s}^{p_{\text{top}}} \omega \frac{\partial h}{\partial p} \frac{dp}{g}. \tag{42}$$

The approximation is due to the fact that the transport of kinetic energy and the horizontal gradient of moist static energy have been neglected. The moist static energy distribution of the 100-hPa simulation is used to compute the energy transport for various hypothetical vertical velocity profiles with $\omega(p) = -\sin[(p_s - p)/(p_s - p_T)]$ for $p > p_T$ and $\omega = 0$ otherwise. The results of this calculation are shown in Fig. 10.

In the equatorial regions, shallow ascent results in a net energy convergence into the atmospheric column. The ascent must rise to 500 hPa or above in order to generate a net energy export. Using the vertical velocity profile from the simulations (shown in Fig. 11) indicates that there is a weak energy convergence in the equatorial regions of the order of 2 kJ kg^{-1}. However, if one restricts the calculation to the ascent occurring below 250 hPa, one finds a very weak energy transport into the convective regions (less than 200 J kg^{-1}). Similar calculations for other latitudes indicate that the ascent in the equatorial jump is associated with very weak energy flow, varying between a net import of 2 kJ kg^{-1} to an export of 2 kJ kg^{-1}, and is thus consistent with a very weak gross moist stability. This contrasts with the ascent regions over the warm SST, which are associated with a strong transport of energy of 12–15 kJ kg^{-1} out of these regions. The weak gross moist stability also implies that the presence of an equatorial jump does not affect the energy transport by the Hadley circulation and, therefore, has a limited impact on the total mass transport.

A fundamental assumption in this argument is that the latent heat of vaporization is converted into sensible heat. This essentially requires precipitation to take place in the ascending regions. Hence, one expects two different behaviors for the equatorial jump, depending on the behavior of convection. On the one hand, in the absence of precipitation, the atmosphere behaves as a dry atmosphere, and exhibits a shallow jump of a few hundred meters above the PBL. In this case, the equatorial jump might be simply associated with a deepening of the PBL. On the other hand, once precipitation is initiated, the ascent must rise above the midtropospheric moist static energy minimum and establish a weak effective stratification.

5. Conclusions

It has been shown here that the depth of the planetary boundary layer can significantly affect the Hadley circulation and the meridional distribution of precipitation. Two different regimes for the cross-equatorial Hadley

[1] An increase in the energy content of the atmosphere must be associated with either an increase in temperature or an increase in the amount of water vapor. On a short time scale, moistening of the lower troposphere can lead to a temperature drop even when the total energy content of the atmosphere increases. On a longer time scale, however, the amount of water vapor is limited by saturation, and the energy content of the atmosphere cannot be increased indefinitely without also increasing the atmospheric temperature.

cell were identified. The first regime occurs for a deep boundary layer and exhibits a single direct cell, with the return flow taking place in the PBL. The second regime occurs for a thin boundary layer, and is characterized by the presence of an ''equatorial jump'': the return flow rises above the PBL in the winter hemisphere, crosses the equator in the free troposphere, and subsides in the PBL on the summer side of the equator. This equatorial jump is associated with a secondary maximum in the precipitation in the winter hemisphere.

This behavior results from dynamical constraints on the PBL flow. In the equatorial regions, the pressure gradients in the free troposphere are particularly weak. The pressure gradient in the ML that is required to sustain any cross-equatorial flow against surface friction must be generated through density gradients within the ML, in a way similar to that discussed by Lindzen and Nigam (1987). The mass transport that can be produced by a given density gradient within the ML is proportional to the third power of the boundary layer thickness. This makes the return flow highly sensitive to the ML dynamics. For a thick ML or a large temperature gradient, a large-enough meridional pressure gradient exists in the equatorial regions to drive a strong cross-equatorial flow. Conversely, for a thin boundary layer, the equator acts as a barrier that forces the return flow to rise above the ML and to cross the equator in the free troposphere.

The equatorial jump occurs in both dry and moist simulations of the cross-equatorial circulation. However, in a dry atmosphere, the return flow barely rises above the ML, while in a moist atmosphere, it rises all the way to the middle troposphere. This difference is viewed as resulting from the weaker gross moist stability in the moist atmosphere due to the compensation between latent heat release and adiabatic cooling. An analysis of the energy transport indicates that the gross moist stability of the equatorial jump is significantly lower than that of moist convective–gravity waves described by Emanuel et al. (1994). It is suggested here that, when precipitation is present, the equatorial jump must rise above the minimum of the moist static energy in the middle atmosphere in order to establish a weak but positive gross moist stability.

In this study, the PBL is represented by a mixed layer of constant thickness. This is a fairly strong simplification, given that the horizontal wind is rarely uniform within the PBL, and that the depth of the PBL varies between less than 100 hPa and more than 200 hPa in the Tropics. Moreover, the idealized radiative forcing used here does not include any cloud–radiative feedbacks. A different representation of the PBL or of the radiation might change the behavior of the cross-equatorial flow, particularly if it affects the transition between nonprecipitating and precipitating convection. For example, in response to dynamical forcing, the PBL might deepen sufficiently near the equator to allow all the return flow to cross the equator within the PBL.

Despite its simplicity, the axisymmetric model points to the central issue of whether the atmosphere can maintain a sufficiently strong cross-equatorial pressure gradient. It might be that, for the current climate, the PBL is deep enough and the SST gradients are large enough so that the Hadley circulation picture is in the classic direct cell regime. However, recent observations by Liu and Xie (2002) indicate the presence of a low-level convergence zone south of the equator in the eastern Pacific. This low-level convergence zone is associated with a weakening of the meridional pressure gradient and meridional wind as the flow approaches the equator, in a way similar to the idealized flows discussed here. Interestingly, this also corresponds to the region where GCMs exhibit a double ITCZ feature. A possible explanation is that these GCMs properly reproduce the dynamical constraints that force the low-level convergence, but they overreact by initiating deep precipitating convection and a deep equatorial jump, while the real atmosphere might only exhibit a weak equatorial jump in the absence of precipitation. These issues require further investigation, but the idealized model clearly indicates that momentum mixing in the PBL can strongly affect the distribution of precipitation in the equatorial regions.

Acknowledgments. Sandrine Bony and Christopher Hill were most helpful in designing the numerical model. I am also thankful to Kerry Emanuel, Isaac Held, and Alan Plumb for our numerous discussions on this topic.

REFERENCES

Adcroft, A., C. Hill, and J. Marshall, 1999: A new treatment of the Coriolis terms in C-grid models at both high and low resolutions. *Mon. Wea. Rev.,* **127,** 1928–1936.

Emanuel, K. A., and M. Zivkovic-Rothman, 1999: Development and evaluation of a convection scheme for use in climate models. *J. Atmos. Sci.,* **56,** 1766–1782.

——, J. D. Neelin, and C. S. Bretherton, 1994: On large-scale circulations in convecting atmospheres. *Quart. J. Roy. Meteor. Soc.,* **120,** 1111–1143.

Fang, M., and K. K. Tung, 1996: A simple model of nonlinear Hadley circulation with an ITCZ: Analytic and numerical solutions. *J. Atmos. Sci.,* **53,** 1241–1261.

Held, I. M., and A. Y. Hou, 1980: Nonlinear axially symmetric circulations in a nearly inviscid atmosphere. *J. Atmos. Sci.,* **37,** 515–533.

Hill, C., and J. Marshall, 1995: Application of a parallel Navier–Stokes model to ocean circulation in parallel computational fluid dynamics. *Parallel Computational Fluid Dynamics: Implementations and Results Using Parallel Computers*, A. Ecer et al., Eds., Elsevier Science, 545–552.

Hou, A. Y., and R. S. Lindzen, 1992: The influence of concentrated heating on the Hadley circulation. *J. Atmos. Sci.,* **49,** 1233–1241.

Lindzen, R. S., and S. Nigam, 1987: On the role of sea surface temperature gradients in forcing low-level winds and convergence in the tropics. *J. Atmos. Sci.,* **44,** 2418–2436.

——, and A. V. Hou, 1988: Hadley circulations for zonally averaged heating centered off the equator. *J. Atmos. Sci.,* **45,** 2416–2427.

Liu, W. T., and X. Xie, 2002: Double intertropical convergence

zones—A new look using scatterometer. *Geophys. Res. Lett.*, **29,** 2072, doi:10.1029/2002GLO15431.

Marshall, J., A. Adcroft, C. Hill, L. Perelman, and C. Heisey, 1997: A finite-volume, incompressible Navier–Stokes model for studies of the ocean on parallel computers. *J. Geophys. Res.*, **102,** 5753–5766.

Neelin, J. D., and I. M. Held, 1987: Modeling tropical convergence based on the moist static energy budget. *Mon. Wea. Rev.*, **115,** 3–12.

Numaguti, A., 1993: Dynamics and energy balance of the Hadley circulation and the tropical precipitation zones: Significance of the distribution of evaporation. *J. Atmos. Sci.*, **50,** 1874–1887.

Pauluis, O., and K. A. Emanuel, 2004: Numerical instability resulting from infrequent calculation of radiative heating. *Mon. Wea. Rev.*, **132,** 673–686.

Peixoto, J. P., and A. H. Oort, 1992: *Physics of Climate.* American Institute of Physics, 520 pp.

Plumb, R. A., and A. Y. Hou, 1992: The response of a zonally symmetric atmosphere to subtropical thermal forcing: Threshold behavior. *J. Atmos. Sci.*, **49,** 1790–1799.

——, and J. Eluszkiewicz, 1999: The Brewer–Dobson circulation: Dynamics of the tropical upwelling. *J. Atmos. Sci.*, **56,** 868–890.

Satoh, M., 1994: Hadley circulations in radiative–convective equilibrium in an axially symmetric atmosphere. *J. Atmos. Sci.*, **51,** 1947–1968.

Schneider, E. K., 1977: Axially symmetric steady-state models of the basic state for instability and climate studies. Part II: Nonlinear calculations. *J. Atmos. Sci.*, **34,** 280–296.

Wheeler, M., and G. N. Kiladis, 1999: Convectively coupled equatorial waves: Analysis of clouds and temperature in the wavenumber-frequency domain. *J. Atmos. Sci.*, **56,** 374–399.

Yu, J.-Y., C. Chou, and J. D. Neelin, 1998: Estimating the gross moist static stability of the tropical atmosphere. *J. Atmos. Sci.*, **55,** 1354–1372.